Abbreviations

%N	percentage nitrogen by mass
2-NDPA	2-Nitrodiphenylamine
AIMD	*ab initio* molecular dynamics
AO	atomic orbital
a.u.	atomic units
B3LYP	Becke, 3-parameter, Lee-Yang-Parr hybrid functional
BCP	bonding critical point
BSSE	basis set superposition error
CH_3/CH_3	NC repeat unit with two $-OCH_3$ capping groups
CH_3/OH	NC repeat unit with $-OCH_3$ capping group on ring 1 and $-OH$ group on ring 2
OH/CH_3	NC repeat unit with $-OH$ capping group on ring 1 and $-OCH_3$ group on ring 2
CCP	cage critical point
CP	critical point
DFT	density functional theory
DFT-D	density functional theory with dispersion correction
DSC	differential scanning calorimetry
DOS	degree of substitution

DPA diphenylamine

EN ethyl nitrate

ESP electrostatic potential

FF force field

G09 Gaussian 09 revision E.01

GGA generalised gradient approximation

GM genetically modified

GTO Gaussian type orbitals

GView Gauss View 5.0.8

HF Hartree-Fock

HMF hydroxymethylfurfural

HOMO highest occupied molecular orbital

IR infra-red spectroscopy

KS-DFT Kohn-Sham DFT

LDA local density approximation

MD molecular dynamics

MEP minimum energy path

MM molecular mechanics

MMFF94 Merck molecular force field 94

MO molecular orbitals

MP2 Møller–Plesset perturbation theory with second order correction

MW molecular weight

NBO natural bond orbital

NC	nitrocellulose
NCP	nuclear critical point
NG	nitroglycerine
NMR	nuclear magnetic resonance spectroscopy
PCM	polarisable continuum model
PES	potential energy surface
PETN	pentaerythritol tetranitrate
PETRIN	pentaerythritol trinitrate
QM	quantum mechanics
QTAIM	quantum theory of atoms in molecules
RCP	ring critical point
RESP	restrained electrostatic potential atomic partial charges
RHF	restricted HF
RMS	root mean square
ROHF	restricted-open HF
UHF	unrestricted HF
SB59	1,4-bis(ethylamino)-9,10-anthraquinone dye
SCF	self-consistent field
SCRF	self-consistent reaction field
SEM	scanning electron microscopy
SMD	solvation model based on density
S_N2	bi-molecular nucleophilic substitution reaction
STO	Slater type orbitals

TG	thermogravitmetric analysis
TS	transition state
UFF	universal force field
UV	ultraviolet
UV-vis	ultraviolet–visible spectroscopy
vdW	van der Waals
ωB97X-D	ωB97X-D long-range corrected hybrid functional
ZPE	zero-point energy

Chapter 1

Post-Denitration Reactions

1.1 Introduction

Products of the preliminary denitration step of nitrocellulose (NC) can be evolved as gases or remain trapped in the polymer matrix. Reactive nitrogen dioxide radicals generated from homolysis of the O-N bond are likely to migrate within the bulk and attack other sites on the polysaccharide, initiating branched radical chain reactions. These lead to deeper decomposition of the polymer *via* chain scission and rupture of glucose rings, with eventual complete disintegration of the molecule, assisted by products released by ongoing acid hydrolysis. Nitrous and nitric acids are released directly from denitration or via transformation of released NO_x species. In addition to catalysing hydrolysis, they increase the acidity of the overall system, lowering the pH and stimulating further hydrolytic processes [1]. The final product mixture is dictated by the numerous side reactions involving autocatalysis, radical reactions and product interactions.

When studying the ageing of NC using ultraviolet–visible spectroscopy (UV-vis), Moniruzzaman *et al.* observed increasing concentrations of reaction products, beyond those generated from first-stage decomposition, with increasing heat treatment and over longer timescales [**?**, 2]. The studies used the reaction of nitrates with an anthraquinone dye (SB59) (figure 1.1) to probe the reactivity at each of the C2, C3 and C6 sites of NC, using ^{1}H NMR spectroscopy and UV-vis (figure 1.2). The reaction of SB59 with NO_x released by denitration (figure 1.3) mimics the action of stabilisers such as diphenylamine (DPA) and 2-Nitrodiphenylamine (2-NDPA) commonly used in NC formulations. The secondary amine groups of the dye consume any nitrates in the system, eliminating the possibility of successive reactions generating acidic species. Un-aged NC thin films, and films aged at 40°C, 50°C, 60°C and 70°C for timescales of up to 2000 hrs for 40°C, were compared.

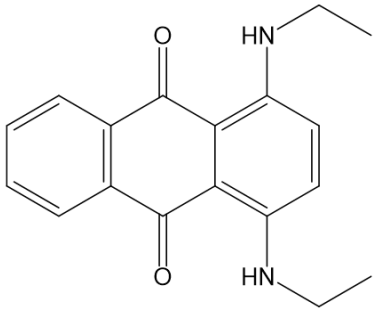

Figure 1.1: 1,4-bis(ethylamino)-9,10-anthraquinone dye (SB59) used to probe the release of nitrates from NC using UV-vis and ^{1}H NMR spectroscopy [2]. The action of nitrate absorption by the dye imitates that of stabilisers commonly used with nitrate ester formulations.

UV absorbances at 600 nm and 650 nm were characteristic of the SB59 dye before reaction with NO_x. The isosbestic point identified at 552 nm showed a proportional relationship between the decrease in concentration of SB59 as it was consumed, with the concentration of the [SB59 + NC] product as it increased.

For samples aged at temperatures >40°C, the isosbestic point demonstrated a downwards shift with increasing dye consumption. The drift from the isosbestic point, in addition to the appearance of new absorbance peaks below 400 nm, allude to the presence of new species in the reaction mixture not generated by the primary reaction of SB59 and NC. It is likely that these arise from the continued reaction of SB59 derivatives with NC degradation products, or further derivatives thereof, as suggested in figure 1.3 III, IV and V. In the case of the 70°C treated run, the final measurement (indicated by the royal-blue line in bold in figure 1.2d)) deviated from the isosbestic point entirely, with more than 81% consumption of the original dye concentration. This suggests that the samples exposed to the higher ageing temperatures presented spectra dominated by products formed *via* secondary reactions.

Following cleavage of the nitrate ester *via* homolytic fission, elimination of HNO_2, or hydrolysis, the resulting residues are available for further reaction with the polymer or other free molecules in the system. In the study of pentaerythritol tetranitrate (PETN) ageing at high temperatures (115°C - 135°C) in vacuum, and low temperatures (20°C - 65°C) in acetonitrile solution, Shepodd *et al.* commented that thermolysis produced a more complex and varied mixture, due to deeper degradation and recombination of radicals [3]. By contrast, the low temperature hydrolytic process emphasised formation of pentaerythritol trinitrate (PETRIN) was followed by side reactions with reduced likelihood of radical re-

(a) NC film aged at 40°C.

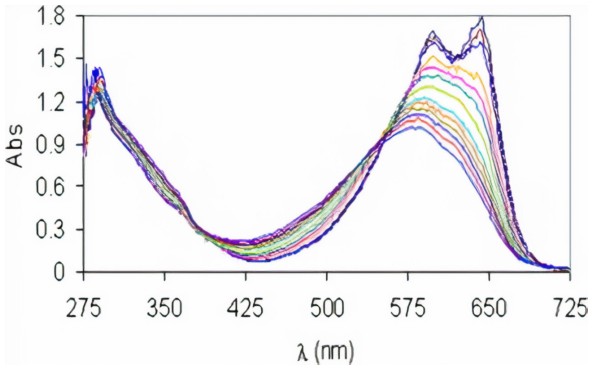

(b) NC film aged at 50°C.

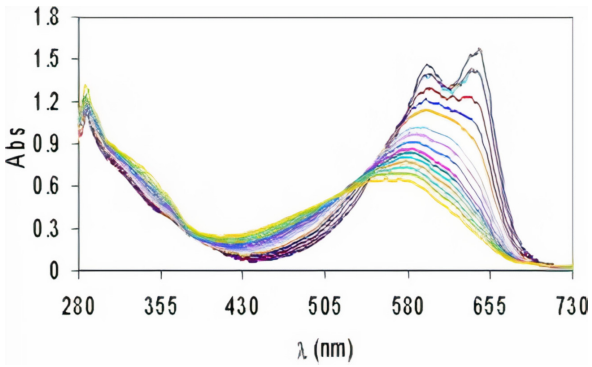

(c) NC film aged at 60°C.

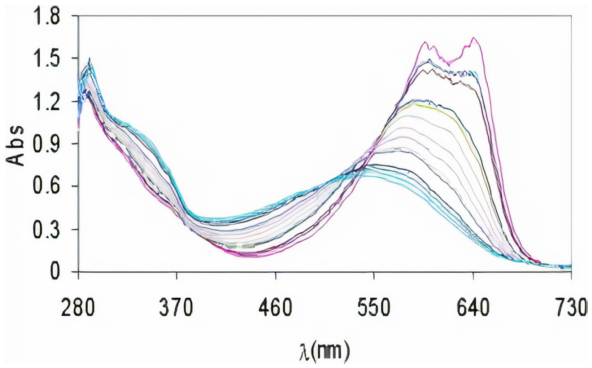

(d) NC film aged at 70°C.

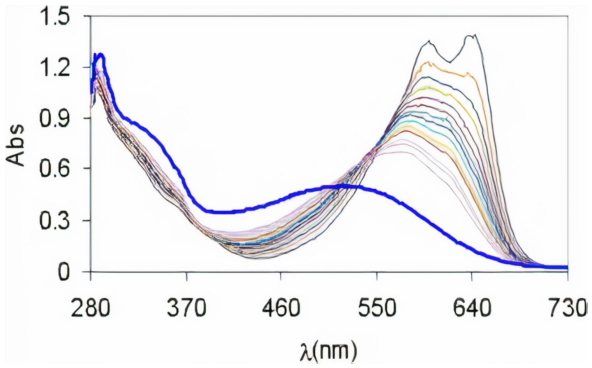

Figure 1.2: UV-vis spectra of aged NC-based film, from the work of Moniruzzaman *et al.*[2]. The peaks at 600 nm and 650 nm are attributed to the π - π* transitions in the anthraquinone dye (SB59). Spectral lines with highest absorbance peaks in this region correspond to the sample prior to heat treatment. Appearance of peaks below 400 nm indicate the formation of new SB59 derivatives due to secondary reactions. Adapted with permission from the publisher.

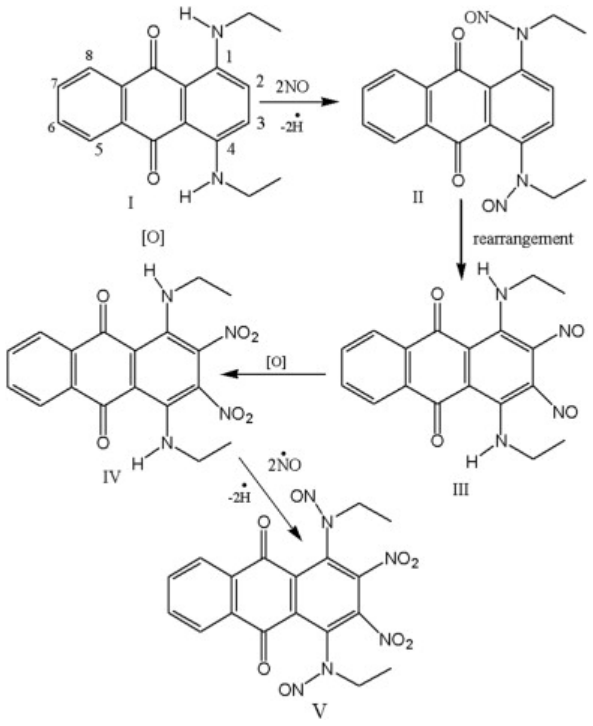

Figure 1.3: Proposed pathway for the reaction of SB59 dye with •NO released as a result of denitration of NC [2]. Reproduced with permission from the publisher.

combination in solution compared to in a solid, as $\bullet NO_2$ would be more likely to diffuse and react elsewhere.

Chin *et al.* proposed schemes for the propagation of secondary reactions initated by both the thermolysis (scheme 1.1) and hydrolysis of nitrate esters (scheme 1.2) [4]. The hydrolysis scheme was adapted from an earlier work by Camera *et al.* involving the nitrate ester decomposition and subsequent reactions of ethyl nitrate (EN) (where R = CH_3CH_2 for the scheme above) [5]. The original study included an expansion of the hydrolysis step (equation 1.11), where the involvement of NO_2^+ was illustrated (scheme 1.3).

It was highlighted by Camera, that the oxidation of alcohol by nitric acid (equation 1.6) is slow and thus rate-limiting. This mechanism is likely to occur *via* a series of intermediate reactions of which the details are not known. However, following the generation of nitrous acid, subsequent oxidations occur rapidly. According to Rigas *et al.*, alcohols are more susceptible to wet oxidation than esters [6]. A higher concentration of unsubstituted hydroxyl groups in the system, and therefore a fewer nitrate ester groups (or a lower degree of substitution (DOS) value), decreases overall stabililty.

Equations 1.7 - 1.10 describe a possible branched radical chain mechanism, fed by the nitrous and nitric acids produced by the hydrolysis and alchohol oxidation reactions during

Scheme 1.1: Thermolytic initiation proposed by Chin *et al.* [4]

$$\mathrm{R{-}ONO_2} \longrightarrow \mathrm{R{-}O\bullet} + \bullet\mathrm{NO_2} \tag{1.1}$$

Propagation

$$\mathrm{R{-}O\bullet} + \bullet\mathrm{NO_2} \xrightarrow{\mathrm{R{-}ONO_2}} \begin{aligned}\mathrm{R{-}ONO_2} &+ \bullet\mathrm{NO} + \bullet\mathrm{NO_2} \\ &+ \mathrm{N_2O_4} + \mathrm{H_2O} + \mathrm{N_2O} \\ &+ \mathrm{CO_2} + \mathrm{CO} + \mathrm{C_2H_2O} \\ &+ \text{other organic fragments}\end{aligned} \tag{1.2}$$

$$2\bullet\mathrm{NO} + \mathrm{O_2} \longrightarrow 2\bullet\mathrm{NO_2} \tag{1.3}$$

$$2\bullet\mathrm{NO_2} \rightleftharpoons \mathrm{N_2O_4} \tag{1.4}$$

Scheme 1.2: Hydrolytic initiation proposed by Chin *et al.* [4]

$$\mathrm{R{-}ONO_2} + \mathrm{H_2O} \longrightarrow \mathrm{R{-}OH} + \mathrm{HNO_3} \tag{1.5}$$

$$\mathrm{R{-}OH} + \mathrm{HNO_3} \longrightarrow \mathrm{R{=}O} + \mathrm{HNO_2} + \mathrm{H_2O} \tag{1.6}$$

Propagation

$$\mathrm{HNO_3} + \mathrm{HNO_2} \rightleftharpoons \mathrm{N_2O_4} + \mathrm{H_2O} \tag{1.7}$$

$$\mathrm{N_2O_4} \rightleftharpoons 2\bullet\mathrm{NO_2} \tag{1.8}$$

$$\mathrm{R{-}OH} + \bullet\mathrm{NO_2} \longrightarrow \bullet\mathrm{R{-}OH} + \mathrm{HNO_2} \tag{1.9}$$

$$\bullet\mathrm{R{-}OH} + \mathrm{HNO_3} \longrightarrow \mathrm{R{=}O} + \mathrm{H_2O} + \bullet\mathrm{NO_2} \tag{1.10}$$

the initiation stage. By contrast, the propagation reactions in the branched radical chain mechanism for thermolysis are poorly characterised (equation 1.2) and defined only by the observable products. Due to their rapid and varied nature, these reactions have been difficult to follow spectroscopically.

Aellig *et al.* presented an alternative scheme for the decomposition of benzyl nitrate (R = $\mathrm{PhCH_2}$) in scheme 1.4, involving more interaction with the solvent [7].Both the Camera/Chin and Aellig schemes above produce final end products observed in the decompo-

Scheme 1.3: Hydrolysis scheme for ethyl nitrate from the work of Camera *et al.* [5]

$$\mathrm{CH_3CH_2ONO_2} + \mathrm{H^+} \overset{\text{fast}}{\rightleftharpoons} \mathrm{CH_3CH_2ONO_2H^+} \tag{1.11}$$

$$\mathrm{CH_3CH_2ONO_2H^+} \overset{\text{slow}}{\rightleftharpoons} \mathrm{CH_3CH_2OH} + \mathrm{NO_2^+} \tag{1.12}$$

$$\mathrm{NO_2^+} + 2\,\mathrm{H_2O} \overset{\text{fast}}{\rightleftharpoons} \mathrm{HNO_3} + \mathrm{H_3O^+} \tag{1.13}$$

sition of NC. In particular, Aellig's scheme accounts for the production of N_2O, which forms a significant part of the decomposition eluent [8]. Whilst the schemes do not a propose an exhaustive description of the full spectrum of reactions that take place in the NC matrix during its slow ageing, the early stage reactions of the key species responsible for decomposition are encapsulated.

Scheme 1.4: HNO_3 decomposition initiation proposed by Aellig *et al.* [7].

$$4\,HNO_3 \rightleftharpoons 4\,{\bullet}NO_2 + 2\,H_2O + O_2 \tag{1.14}$$

$$2\,{\bullet}NO_2 + H_2O \rightleftharpoons N_2O_4 + H_2O \tag{1.15}$$

$$N_2O_4 + H_2O \longrightarrow HNO_3 + HNO_2 \tag{1.16}$$

Propagation

$$R{-}OH + HNO_2 \rightleftharpoons R{-}ONO + H_2O \tag{1.17}$$

$$R{-}ONO \longrightarrow R{=}O + HNO \tag{1.18}$$

$${\bullet}NO_2 + HNO \longrightarrow HNO_2 + {\bullet}NO \tag{1.19}$$

$$2{\bullet}NO + O_2 \longrightarrow 2{\bullet}NO_2 \tag{1.20}$$

Termination

$$2\,HNO \longrightarrow HON{=}NOH \tag{1.21}$$

$$HON{=}NOH \longrightarrow N_2O + H_2O \tag{1.22}$$

It is widely agreed that first-stage decomposition follows a first-order process (or pseudo-first order, with respect to hydrolysis reactions). A number of studies observe catalytic rate of decay for the longer-term aging processes. Dauerman and Tajima [9] observed that when NC was treated with NO_2 gas before heating, the time required for sample ignition halved. He suggested that the NO_2 adsorbed onto the surface acted as a catalysing agent.

Neutral and alkaline hydrolysis reactions follow a pseudo-first order process, however it has been suggested that the presence of acid facilitates a catalytic rate of degradation after an initial incubation period. Multiple studies have addressed the decomposition reactions of nitrate esters following the initial scission of the nitrate group [1, 5, 10, 11, 12]. In their work looking into the atmospheric reactions of methynitrate and methylperoxy nitrate Arenas *et al.* suggested it was possible for the homolytic denitration reaction of methynitrate to share a common peroxy intermediate with the peroxide [**?**]. This could account for some of the lower order NO_x generated. In this section, secondary and extended reaction schemes

for the low temperature ageing of NC are explored. Decomposition pathways defined by Chin, Camera *et al.* and Aellig *et al.* are probed to determine the reactions responsible for the experimentally observed degradation products. The reactions found to be energetically feasible from the proposed routes will be scrutinised to determine whether an autocatalytic pathway can be formed from the thermodynamically validated reaction schemes.

1.2 Methodology

The reactions proposed by Chin *et al.*, Camera *et al.* and Aellig *et al.* were used to construct possible degradation routes for NC, each route starting with either the products of homolytic fission, elimination of HNO_2 or acid hydrolysis. The energies of each reaction in the schemes above were determined after optimisation of the individual reactant and product species. Pathways were constructed based on propagation of the given reactions in a stepwise fashion; subsequent reactions were dependent on the products generated in preceding steps. An abundance of water and oxygen were assumed present in the system, attributed to air exposure under the wetted storage conditions of NC. Unsubstituted alcohol moieties (R-OH) were also presumed abundant due to incomplete nitration during the synthesis of NC [**?**], and re-generation following denitration *via* hydrolysis. The schemes were modelled with ethyl nitrate (EN) as a smaller test system, then expanded to the NC monomer. Free energies of reaction (ΔG_r) at 298.15 K were used to determine the feasibility of each reaction:

$$\Delta G_r = \Delta G_{product} - \Delta G_{reactant} \tag{1.23}$$

Where computational or experimental literature values for molecular energies or for reactions energies were available, these were compared with the results generated here. For the cases where the ΔG_r was large and positive, the reaction was omitted from the constructed reaction schemes as it would be unlikely to occur spontaneously under ambient ageing conditions, even when considering the possibility of increased heating in the system as degradation progressed.

1.2.1 Computational details

All geometry optimisations were conducted in Gaussian 09 revision E.01 (G09), using the ωB97X-D and B3LYP functionals. Optimisations and thermochemistry calculations were performed to the level of 6-31+G(2df,p) with tight convergence criteria (max. force 1.5×10^{-5} H/Bohr, RMS force 1.0×10^{-5}, max. displacement 6.0×10^{-5} H/Bohr and RMS

displacement 4.0×10^{-5} H/Bohr, chapter **??** table **??**) and zero point energy corrected. Calculations were repeated in both vacuum and with a polarisable continuum model (PCM) using water (ε=78.4) to introduce implicit solvent effects. Chemical species were constructed using Gauss View 5.0.8 (GView) [13] and for molecules of more than 3 atoms, the GView "Clean" function was used to re-order atoms to a preliminary starting geometry. Energies of optimised structures were checked against literature values listed on NIST Computational Chemistry Comparison and Benchmark Database [14] if analogous molecules to a similar level of theory existed. In most cases, the exact same level of theory was not available but a similar level could still be meaningfully referenced; for example, ωB97X-D / 6-31G(d,p) instead of ωB97X-D / 6-31+G(2df,p) was available for most of the common small molecules. These comparisons are detailed alongside the calculated energies in the text.

1.3 Results and Discussion

Individual molecules were optimised and their energies were calculated to evaluate the ΔG for each of the reactions in schemes 1.1-1.4 proposed by Chin *et al.*, Camera *et al.* and Aellig *et al.*. The protonation of EN was inspected to determine whether the protonation site matched that of NC, where the bridging site was the most likely to lead to hydrolytic denitration. This would indicate that EN followed the same hydrolytic mechanism, and was therefore likely to share the same extended decomposition scheme initiated by hydrolysis. The proton was placed at each of the possible terminal and bridging sites around the nitrate, and the energy for each isomer was calculated. Table 1.1 shows the protonation energies for the three different oxygen sites on EN. Despite the terminal (syn) oxygen possessing the most thermodynamically favourable energy of protonation, inspection of the reaction geometries (figure 1.4) shows that the bridging structure most resembles that expected for the liberation of the NO_2^+ group at the next step, as was observed in the case of NC (section **??**). The higher $\Delta G_{proton.}$ arises from the elongation of the O$-$NO$_2$ bond that allows stabilisation of the bridging site, whilst preparing to lose the NO_2^+. Further studies involving protonated EN used the values and geometry associated with the protonated bridging site.

The combined list of calculated energies for the reactions in all schemes, for both EN and the NC monomer, are listed in table 1.2. The obtained energies for the formation of N_2O_4 from 2•NO_2 were are out of the experimentally recorded range of 4.7 - 5.9 kcal mol^{-1} [15] (from calculation: ωB97X-D/ 6-31+G(2df,p) ΔG_r = 0.1 kcal mol^{-1} in vacuum and 1.5

Table 1.1: Free energies of protonation for each oxygen site on EN.

Protonated site		$\Delta G_{proton.}$ /kcal mol^{-1}			
		ωB97X-D	PCM	B3LYP	PCM
Terminal (syn)	$CH_3CH_3ONO_2H^+$	−12.3	8.8	−13.8	5.6
Terminal (anti)	$CH_3CH_3ONO_2H^+$	−9.5	9.5	−11.1	5.6
Bridging	$CH_3CH_3O(H^+)NO_2$	−9.3	9.1	−15.3	6.7

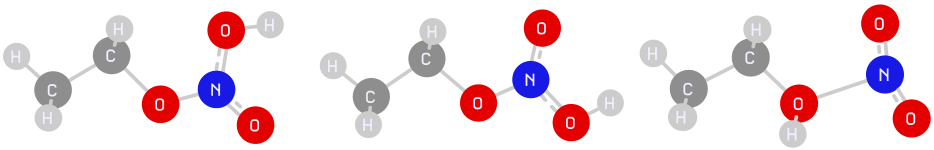

(a) Syn terminal oxgen. Bond(O–NO_2): 1.28 Å

(b) Anti terminal oxgen. Bond(O–NO_2): 1.28 Å

(c) Bridging oxgen. Bond(O–NO_2): 1.98 Å

Figure 1.4: Optimised geometries of the possible protonation sites on EN.

kcal mol^{-1} in water, and B3LYP/ 6-31+G(2df,p), ΔG_r = -0.5 kcal mol^{-1} in vacuum and -0.2 kcal mol^{-1} in water). The B3LYP result incorrectly predicts that the reaction is spontaneous under ambient conditions. This error may arise from a number of factors, including the limitation to short-range interactions in B3LYP, the general tendency of density functional methods to under predict reaction energies, or the geometry optimisation procedure, whereby a small variation or imperfect minimisation in the obtained optimised structures for the reaction species is amplified when combined for the calculation of reaction energies.

For the reaction of $HNO_3 + HNO_2 \rightleftharpoons N_2O_4 + H_2O$ in the gas phase, ωB97X-D/ 6-31+G(2df,p) gave ΔG_r = -2.2 kcal mol^{-1} and B3LYP/ 6-31+G(2df,p) gave ΔG_r = -5.1 kcal mol^{-1}. The corresponding published theoretical reaction energies calculated at ωB97X-D/ 6-31+G(d,p) and B3LYP/ 6-31+G(d,p) were -1.0 kcal mol^{-1} and -4.3 kcal mol^{-1} respectively. The literature and calculated values cannot be directly cross-referenced as the applied basis sets differ, however it can be seen that in either set there is a large relative disparity between the two functionals. Values are lower for B3LYP likely as a result of neglect of mid to long-range correlations that have been included in ωB97X-D; it is therefore expected for the B3LYP result to more heavily underpredict reaction energies when these interactions are signficant in the studied system [16]. This is illustrated in the energies of N_2O_4, where the long-range interaction of each nitrogen with oxygens of the other nitrogen group are missed, and the B3LYP/ 6-31+G(2df,p) energy falls below the ωB97X-D energy by 89 kcal mol^{-1}.

Table 1.2: Calculated energies for the nitrate ester decomposition reactions proposed by Camera *et al.*, Chin *et al.* and Aellig *et al.* [5, 4, 7]. R = CH_3CH_2 for ethyl nitrate (EN), and R = $(H_3CO)_2C_6H_9O_3$ (bi-methoxy capped glucopyraonse monomer unit) for NC. The PCM model applied was water ($\varepsilon = 78.4$).

Reaction	ΔG_r /kcal mol^{-1}			
	ωB97X-D	PCM	B3LYP	PCM
$N_2O_4 + H_2O \longrightarrow HNO_3 + HNO_2$	2.3	1.9	5.1	4.2
$N_2O_4 \rightleftharpoons 2{\bullet}NO_2$	0.1	1.5	−0.5	−0.2
Radical reactions				
${\bullet}NO_2 + HNO \longrightarrow HNO_2 + {\bullet}NO$	−28.2	−28.7	−27.3	−27.6
$2{\bullet}NO + O_2 \longrightarrow 2{\bullet}NO_2$	−20.8	−22.0	−21.2	−22.2
Acid reactions				
$HNO_3 + HNO_2 \rightleftharpoons N_2O_4 + H_2O$	−2.2	−1.8	−5.1	−4.2x
$4\,HNO_3 \rightleftharpoons 4{\bullet}NO_2 + 2\,H_2O + O_2$	53.4	58.4	42.6	46.9
$2\,HNO \longrightarrow HON{=}NOH$	−39.0	−39.7	−36.6	−37.4
$HON{=}NOH \longrightarrow N_2O + H_2O$	−48.1	−48.2	−50.6	−50.7
Ionic reactions				
$NO_2^+ + 2\,H_2O \rightleftharpoons HNO_3 + H_3O^+$	−0.9	−1.3	1.8	2.5
EN (R = CH_3CH_2)				
$R{-}ONO_2 + H_2O \longrightarrow R{-}OH + HNO_3$	4.6	5.2	4.0	4.9
$R{-}OH + HNO_3 \longrightarrow R{=}O + HNO_2 + H_2O$	−34.1	−38.4	−37.6	−41.8
$R{-}OH + {\bullet}NO_2 \longrightarrow {\bullet}R{-}OH + HNO_2$	16.4	13.9	15.9	13.7
${\bullet}R{-}OH + HNO_3 \longrightarrow R{=}O + H_2O + {\bullet}NO_2$	−50.4	−52.4	−53.5	−55.5
$R{-}OH + HNO_2 \rightleftharpoons R{-}ONO + H_2O$	−3.2	−3.3	−2.6	−2.9
$R{-}ONO \longrightarrow R{=}O + HNO$	−1.5	−5.8	−4.4	−8.5
NC monomer (R = $(H_3CO)_2C_6H_9O_3$)				
$R{-}ONO_2 + H_2O \longrightarrow R{-}OH + HNO_3$	0.7	5.6	0.6	−0.7
$R{-}OH + HNO_3 \longrightarrow R{=}O + HNO_2 + H_2O$	−36.7	−38.3	−41.7	−41.7
$R{-}OH + {\bullet}NO_2 \longrightarrow {\bullet}R{-}OH + HNO_2$	14.7	11.2	13.0	23.2
${\bullet}R{-}OH + HNO_3 \longrightarrow R{=}O + H_2O + {\bullet}NO_2$	−51.4	−49.5	−54.7	−56.4
$R{-}OH + HNO_2 \rightleftharpoons R{-}ONO + H_2O$	−4.4	−7.3	−4.3	−0.2
$R{-}ONO \longrightarrow R{=}O + HNO$	−2.9	−1.7	−6.8	−11.2

Simplified schemes for the possible ageing reactions of nitrate esters beginning from homolytic fission, elimination of HNO_2 or acid hydrolysis are illustrated in schemes 1.5 - 1.7. The reaction of $4\,HNO_3 \rightleftharpoons 4\,{\bullet}NO_2 + 2\,H_2O + O_2$ has a large, positive ΔG_r of 53.4 kcal mol^{-1} (ωB97X-D/ 631+G(2df,p) in vacuum) indicating that this process is highly unlikely to proceed in given ambient temperatures, and so was omitted from the drawn reaction schemes.

When starting with the products of homolytic fission (scheme 1.5), the reaction pathway split into a branched radical chain mechanism and separate acid driven pathway. Reaction of $\bullet NO_2$ with a hydroxyl group (on either the NC monomer or denitrated EN molecule) leads to the formation of an alkyl radical which goes on to react with HNO_3 present in the environment from formation *via* other steps in the pathway, formed during the reaction of NO_2^+ in the hydrolytic scheme, or residual in the system from incomplete washing following NC synthesis, to regenerate $\bullet NO_2$. The $\bullet NO_2$ attack on R−OH is expected to occur rapidly, dominating the reaction scheme but leading to increased concentration of $\bullet NO_2$ in the system to fuel other pathways. Formation of N_2O_4 from $2\bullet NO_2$ and subsequent decomposition into HNO_2 and HNO_3 drives the remaining acid reactions. HNO_3 reactions lead to further formation of $\bullet NO_2$, however, the attack of HNO_2 on hydroxyl groups on the NC backbone generates the experimentally observed end product N_2O whilst the hydroxyl group is converted to a ketone [9, 17].

The generation and re-generation of $\bullet NO_2$ and HNO_2 in the above scheme supports the theory that these may be the species responsible for the autocatalytic rate of decomposition that is observed following a first-order rate induction period [18, 19, 20]. The first-order rate is likely attributed to the denitration step, as the concentration of these species slowly increases and self-heating occurs, leading to the rapid speed-up of the post-denitration reactions. If the liberated HNO_2 does not go on to attack hydroxyl groups on the NC backbone, it is then free to undergo a conversion to generate further $\bullet NO_2$ in the reactions $HNO_2 + HNO_3 \longrightarrow N_2O_4 + H_2O \rightleftharpoons 2\bullet NO_2$ +H2O, indicating that the fate of all nitrogen in the system is towards the formation of $\bullet NO_2$ until it is captured in N_2O. This is supported by scheme 1.6 that begins with the elimination of HNO_2. The reactions of HNO_2 with available hydroxyl groups drives the formation of N_2O, ketone and water as the only end products. The hydrolytic scheme (scheme 1.7) involves the early generation of HNO_3, conversion to HNO_2 and then enters a similar radical chain mechanism to that observed in

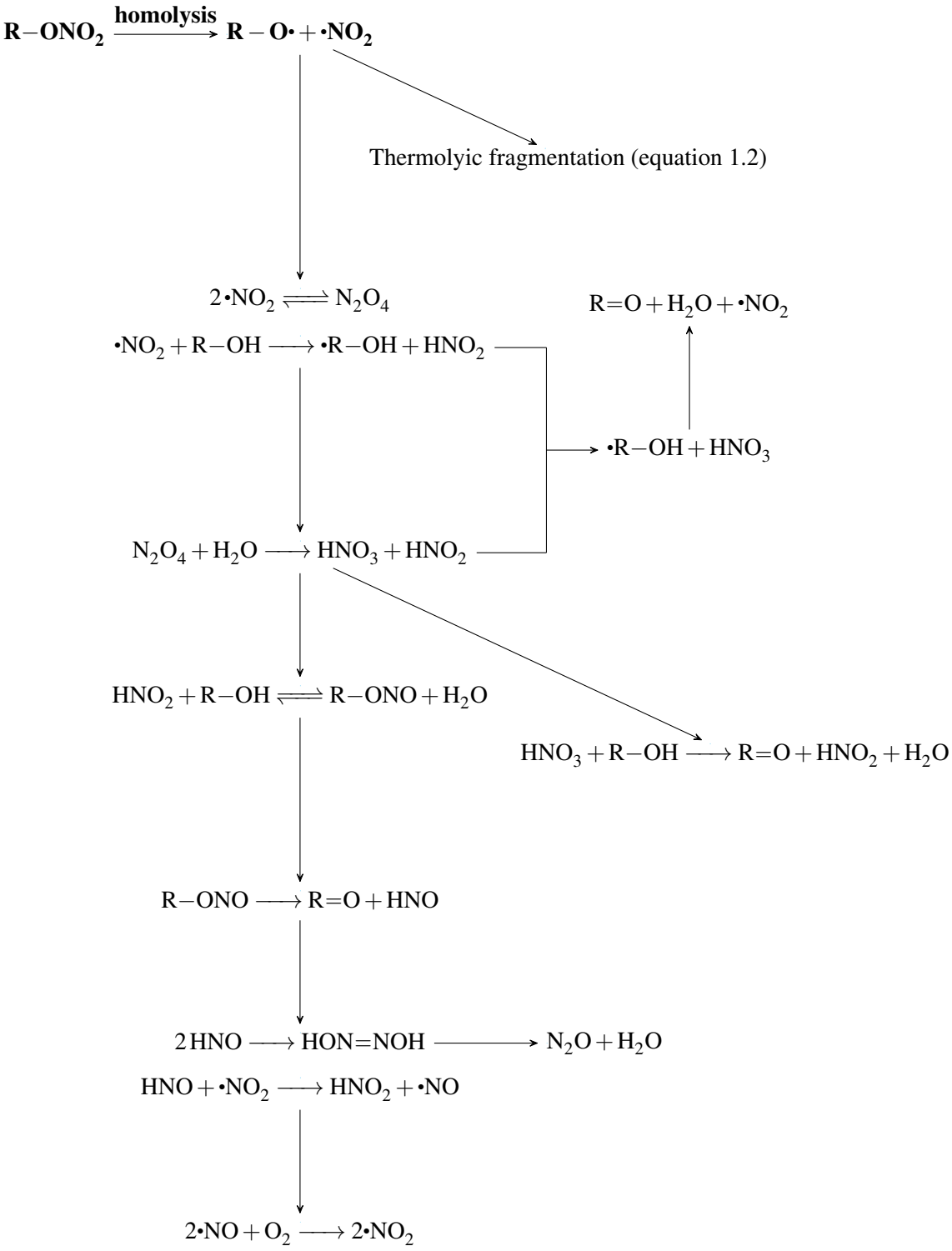

Scheme 1.5: Proposed degradation pathway starting from the homolytic fission of the nitrate ester, derived from the schemes presented by Camera *et al.* [5] and Aellig[7].

the homolytic pathway concluding in formation of N_2O, $\bullet NO_2$ and hydroxyl conversion to ketone. For all schemes, R=O and N_2O were terminating species. Whilst N_2O is released into the environment, R=O remains in the system may go on to participate in further decomposition reactions leading to ring opening. It is important to note that these schemes are not exhaustive, but rather a limited view of the possible steps that may take place during ageing based on the presence of nitrate and acid species expected to be in the closed system. Deeper degradation of the NC backbone has not been considered here and should the next step for future work.

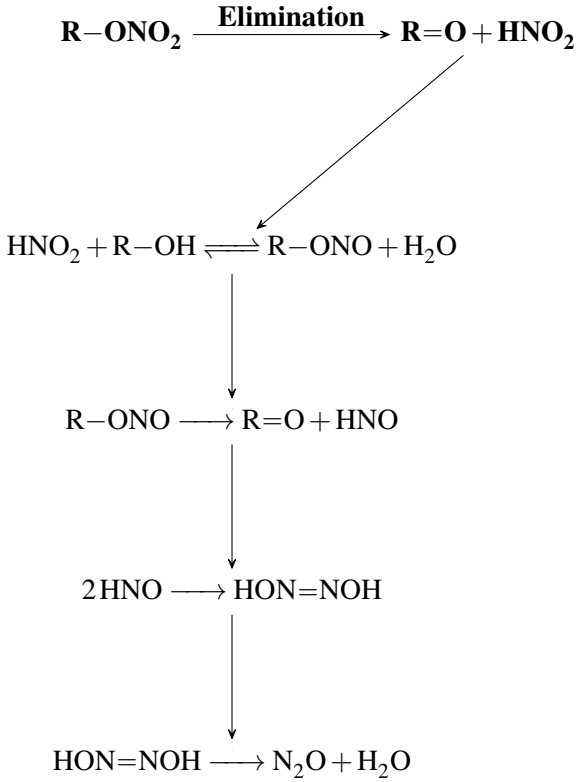

Scheme 1.6: Proposed degradation pathway starting from the elimination of HNO_2 from a nitrate ester, derived from the schemes presented by Camera *et al.* [5] and Aellig[7].

1.4 Summary

In this section, the energies (ΔG_r) for each of the reactions in the combined nitrate ester decomposition schemes proposed by Camera *et al.*, Chin *et al.* and Aellig *et al.* were evaluated using the ωB97X-D and B3LYP functionals [5, 4, 7]. Obtained energy values were compared to literature where available [14], confirming that individual molecular free energy and reaction energy values fell within the expected theoretical and experimental bounds. Decomposition reactions involving an alkyl nitrate were initially performed with

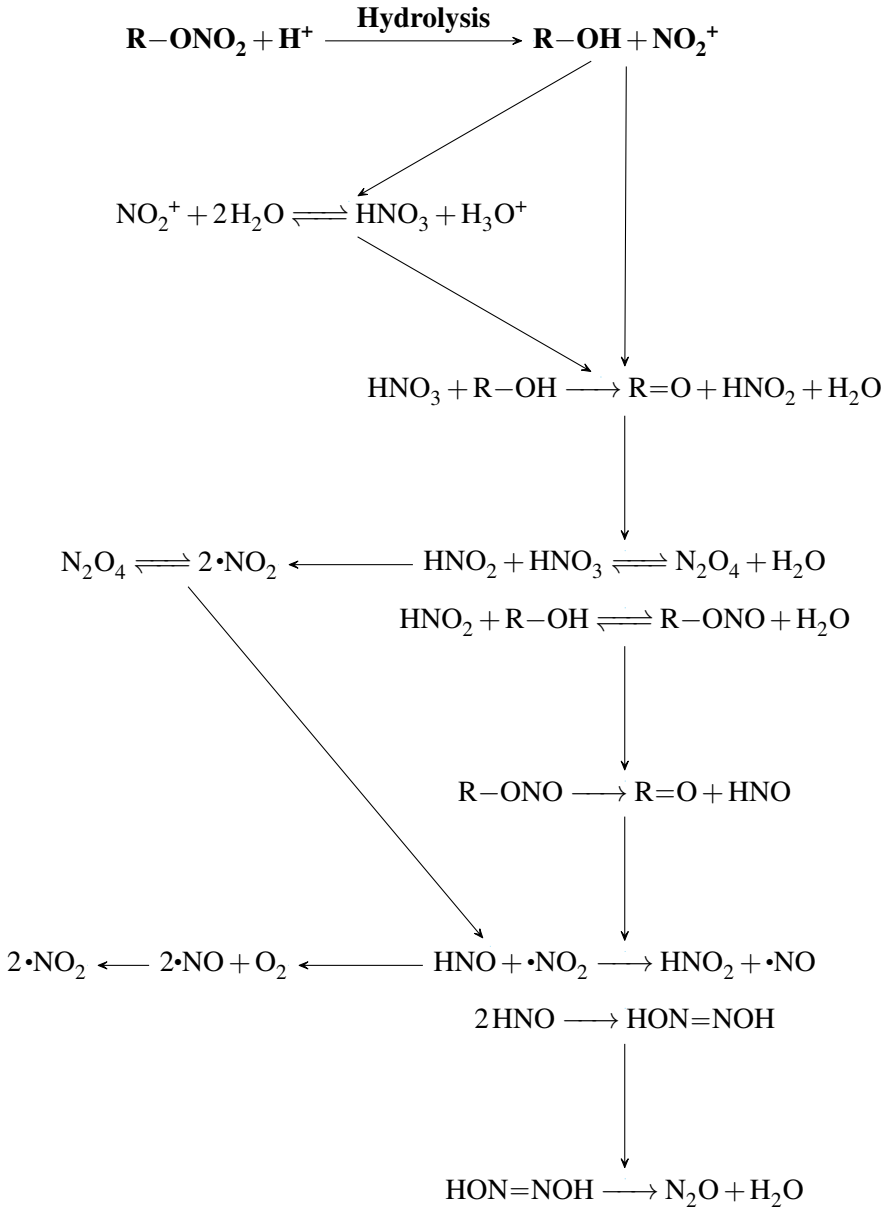

Scheme 1.7: Proposed degradation pathway starting from the acid hydrolysis of a nitrate ester, derived from the schemes presented by Camera *et al.* [5] and Aellig[7].

ethyl nitrate (EN) and then repeated for NC.

Starting from the three denitration mechanisms explored in chapter **??**, using the reactions listed in the schemes above, three different degradation pathways were constructed.

It can be seen that it is the HNO_2 species conversion of $R-OH \rightarrow R-ONO \rightarrow R=O$ that drives oxidation in all three schemes, playing a central role in the extended degradation scheme of NC. The regeneration of $\bullet NO_2$ indicated that this was the species most likely responsible for the autocatalytic rate of degradation observed experimentally [21, 22, 23].

Decomposition further than formation of the ketone species was not studied here. To understand the full ageing behaviour of NC and comprehensively attribute experimentally observed products to individual reactions, the relative rate of each of the mechanistic schemes above, in addition to ring fission and peeling-off reactions that disrupt the NC chain, must be probed. A limitation to this work is that the reaction energies were calculated from the molecules optimised in isolation. In practice, there are energy barriers associated with complexation of reactant compounds and solvation energies as newly liberated species depart from the NC backbone to freely move in the solvent. To account for these, a more detailed study to evaluate complexation and solvation energies is needed. The diffusion behaviour of individual reactant species through the NC bulk both in vacuum and solvent, and as the reaction mixtures evolves, should also be considered.

Bibliography

[1] K. S. Hu, A. I. Darer, and M. J. Elrod. Thermodynamics and kinetics of the hydrolysis of atmospherically relevant organonitrates and organosulfates. *ACP*, 11(16):8307–8320, August 2011.

[2] Mohammed Moniruzzaman, John M. Bellerby, and Manfred A. Bohn. Activation energies for the decomposition of nitrate ester groups at the anhydroglucopyranose ring positions c2, c3 and c6 of nitrocellulose using the nitration of a dye as probe. *Polymer Degradation and Stability*, 102:49–58, 2014.

[3] T. Shepodd, R. Behrens, D. Anex, D. Miller, and K. Anderson. Degradation chemistry of petn and its homologues. Technical report, Sandia National Laboratories, United States, 1997.

[4] Anton Chin, Daniel S. Ellison, Sara K. Poehlein, and Myong K. Ahn. Investigation of the decomposition mechanism and thermal stability of nitrocellulose/nitroglycerine based propellants by electron spin resonance. *Propellants, Explosives, Pyrotechnics*, 32(2):117–126, April 2007.

[5] E. Camera, G. Modena, and B. Zotti. On the behaviour of nitrate esters in acid solution. ii. hydrolysis and oxidation of nitroglycol and nitroglycerin. *Propellants, Explosives, Pyrotechnics*, 7(3):66–69, June 1982.

[6] Fotis Rigas, Ioannis Sebos, and Danae Doulia. Safety charts simulation of nitroglycerine/nitroglycol spent acids via chemical reaction kinetics. *Ind. Eng. Chem. Res.*, 36(12):5068–5073, December 1997.

[7] Christof Aellig, Ulrich Neuenschwander, and Ive Hermans. Acid-catalyzed decomposition of the benzyl nitrite intermediate in hno3-mediated aerobic oxidation of benzyl alcohol. *ChemCatChem*, 4(4):525–529, April 2012.

[8] S. J. Buelow, D. Allen, G. K. Anderson, F. L. Archuleta, J. H. Atencio, G. T. Baca, W. D. Breshears, T. J. Butenhoff, P. C. Dell'Orco, R. B. Dyer, B. R. Foy, K. A. Funk, D. M. Harradine, K. C. Knutsen, J. L. Lyman, D. A. Masten, T. G. McGuinness, R. E. McInroy, C. J. Monahan, R. C. Oldenborg, J. M. Robinson, M. A. Sedillo, D. A. Counce, C. K. Rofer, P. E. Trujillo, R. L. Brewer, G. A. Buntain, R. L. Flesner, J. A. Sanchez, T. Spontarelli, L. L. Sprouse, C. A. Vecere, G. R. Brewer, R. D. McFarland, W. J. Parkinson, R. P. Courier, S. M. Chitanvis, C. W. Pattersen, and L. R. Pratt. Destruction of energetic materials in supercritical water. Technical report, Air Force Research Laboratory, Los Alamos National Laboratory, New Mexico 87545, 2002.

[9] L. Dauerman and Y. A. Tajima. Thermal decomposition and combustion of nitrocellulose. *AIAA Journal*, 6(8):1468–1473, August 1968.

[10] E. Camera, G. Modena, and B. Zotti. On the behaviour of nitrate esters in acid solution. iii. oxidation of ethanol by nitric acid in sulphuric acid. *Propellants, Explosives, Pyrotechnics*, 8(3):70–73, June 1983.

[11] John W. Baker and D. M. Easty. 217. hydrolytic decomposition of esters of nitric acid. part i. general experimental techniques. alkaline hydrolysis and neutral solvolysis of methyl, ethyl, isopropyl, and tert.-butyl nitrates in aqueous alcohol. *J. Chem. Soc.*, (0):1193–1207, 1952.

[12] V. G. Matveev and G. M. Nazin. Stepwise degradation of polyfunctional compounds. *Kinetics and Catalysis*, 44(6):735–739, 2003.

[13] Roy Dennington, Todd A. Keith, and John M. Millam. Gaussview Version 5.0.8, 2009. Semichem Inc. Shawnee Mission KS.

[14] NIST Computational Chemistry Comparison and Benchmark Database. Nist standard reference database number 101. http://cccbdb.nist.gov/, August 2020.

[15] Neha Awasthi, Thomas Ritschel, Reinhard Lipowsky, and Volker Knecht. Standard gibbs energies of formation and equilibrium constants from ab-initio calculations: Covalent dimerization of no2 and synthesis of nh3. *The Journal of Chemical Thermodynamics*, 62:211–221, 2013.

[16] Jeng-Da Chai and Martin Head-Gordon. Long-range corrected hybrid density functionals with damped atom-atom dispersion corrections. *Phys. Chem. Chem. Phys.*, 10(44):6615–6620, 2008.

[17] G. K. Adams and C. E. H. Bawn. The homogeneous decomposition of ethyl nitrate. *Trans. Faraday Soc.*, 45(0):494–499, 1949.

[18] I. Rodger and J. D. Mcirvine. The decomposition of spent petn nitration acids. *Can. J. Chem. Eng.*, 41(2):87–90, April 1963.

[19] Torbjörn Lindblom. Reactions in stabilizer and between stabilizer and nitrocellulose in propellants. *Propellants, Explosives, Pyrotechnics*, 27(4):197–208, September 2002.

[20] Hermann N. Volltrauer and Arthur Fontijn. Low-temperature pyrolysis studies by chemiluminescence techniques real-time nitrocellulose and pbx 9404 decomposition. *Combustion and Flame*, 41:313–324, 1981.

[21] N. Binke, L. Rong, Y. Zhengquan, W. Yuan, Y. Pu, Hu Rongzu, and Y. Qingsen. Studies on the kinetics of the first order autocatalytic decomposition reaction of highly nitrated nitrocellulose. *Journal of Thermal Analysis and Calorimetry*, 58(2):403–411, 1999.

[22] Kai Wang, Dabin Liu, Sen Xu, and Gaowen Cai. Research on the thermal history's influence on the thermal stability of ehn and nc. *Thermochimica Acta*, 610:23–28, 2015.

[23] Hua Chai, Qiangling Duan, Lin Jiang, Liang Gong, Haodong Chen, and Jinhua Sun. Theoretical and experimental study on the effect of nitrogen content on the thermal characteristics of nitrocellulose under low heating rates. *Cellulose*, 26(2):763–776, 2019.